Electronic Supplementary Material (ESI) for Dalton Transactions.

Supplementary Materials for

Highly selective electrocatalytic reduction of CO_2 to HCOOH over an in-situ derived Ag-loaded $Bi_2O_2CO_3$ electrocatalyst

Wei Zheng,‡[a] Changlai Wang,‡[a] Jing Chen,[a] Shi Chen,[a] Zhiyu Lin,[a] Minxue Huang,[a] Hao Huang,[a] Yafei Qu,[a] Peichen Wang,[a] Lin Hu,*[b] and Qianwang Chen*[ab]

Materials and Methods.

Chemicals: All chemicals were directly used without further purifications. Bismuth nitrate pentahydrate ($Bi(NO_3)_3{\cdot}5H_2O$), silver nitrate ($AgNO_3$), potassium bicarbonate ($KHCO_3$), potassium hydroxide (KOH), ethanol (CH_3CH_2OH) were purchased from Sinopharm Chemical Reagent Co., Ltd (Shanghai, China). Nafion perfluorinated resin solution (5wt% in lower aliphatic alcohols and water) and Nafion® N-117 membrane (0.18 mm thick) were purchased from Sigma-Aldrich.

Preparation of Bi_2O_3: Bi_2O_3 was synthesized by the hydrothermal method. Firstly, 727.6 mg of $Bi(NO_3)_3{\cdot}5H_2O$ (1.5 mmol) was dissolved in 10 mL of 2 mol L^{-1} HNO_3 aqueous solution, sonicated, and stirred until clear. Then, 1 mL of glycerol was added to the mixture and stirred at room temperature for 10 min, followed by the addition of a 2.5 mol L^{-1} NaOH solution to adjust the pH of the solution to 8.5. After stirring for another 10 min, the resulting mixture was transferred to a 50 mL poly(tetrafluoroethylene) (PTFE)-lined stainless-steel autoclave, heated to 160℃ for 1 h, and cooled at room temperature naturally after that. The precipitate was centrifuged and washed several times with distilled water and absolute ethanol, and then dried at 60℃ for 12 h. The resulting powder sample was stored for further use.

Preparation of Ag/Bi_2O_3: Ag/Bi_2O_3 was prepared by deposition-precipitation method. Firstly, a Bi_2O_3 aqueous suspension (100 mg in 20 mL H_2O) was sonicated for 10 min. 10mL of $AgNO_3$ solution (1 mg/mL) was added dropwise to the Bi_2O_3 aqueous suspension under vigorous stirring for 1 h. Then 5 mL of a 0.1 M NaOH aqueous solution was added into it. After that, it was centrifuged and washed with deionized water until the pH value of the supernatant was neutral. The precipitate was filtered and dried at 70°C overnight. Then the resulting powder was heated at a ramping rate of 5℃ min^{-1} to 450℃ and maintained at the temperature for 1 hour in the air. The product was cooled down to room temperature after that, denoted as Ag/Bi_2O_3-1. By changing the volume of $AgNO_3$ solution into 2mL and 10mL, we can synthesize samples with different Ag loadings, denoted as Ag/Bi_2O_3-2 and Ag/Bi_2O_3-3, respectively.

Preparation of working electrode: 4 mg Ag/Bi_2O_3 and 30 μL Nafion solution (5%) were dispersed into 970 μL ethanol under sonication for 1 h to form a homogeneous catalyst ink. The working electrode was prepared by dropping 125 μL of catalyst ink onto carbon fiber paper (1 cm × 1 cm). Then constant-potential electrolysis in CO_2-saturated 0.5 M $KHCO_3$ under -0.9 V was performed for 30 min to transform the pre-catalyst Ag/Bi_2O_3 into $Ag/Bi_2O_2CO_3$. The $Ag/Bi_2O_2CO_3$ transformed from Ag/Bi_2O_3-1, Ag/Bi_2O_3-2 and Ag/Bi_2O_3-3 were denoted as s-1, s-2 and s-3. Similarly, $Bi_2O_2CO_3$ can be synthesized by Bi_2O_3 using the same method.

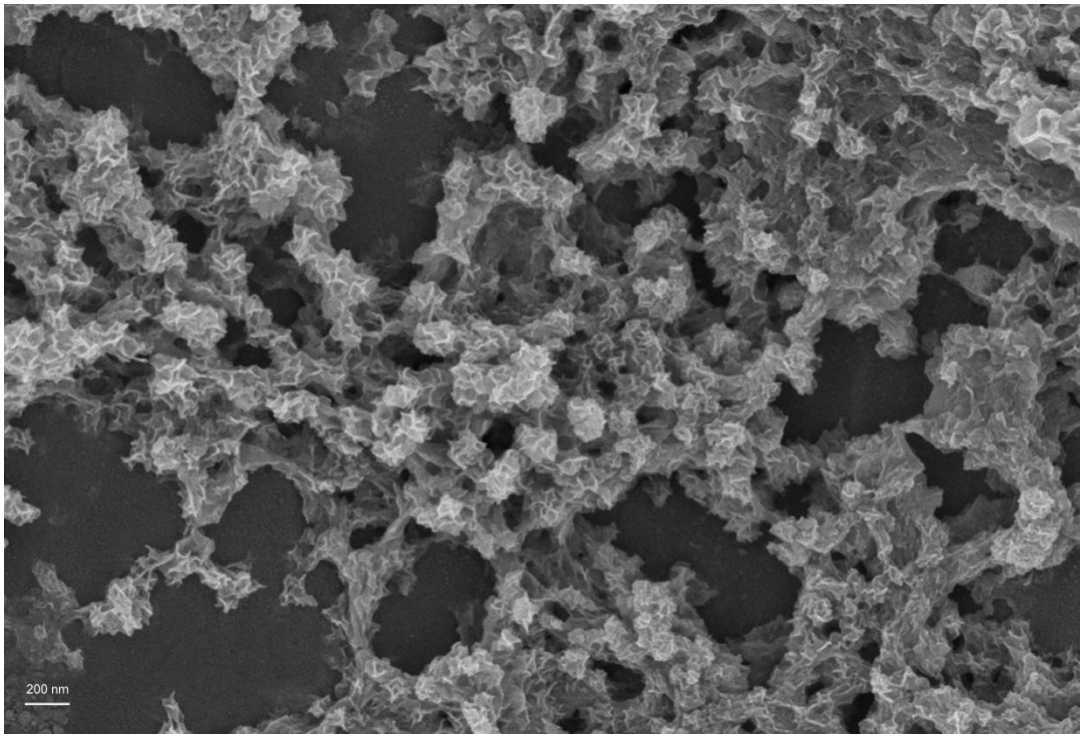

Fig. S1. The SEM image of Ag/Bi_2O_3.

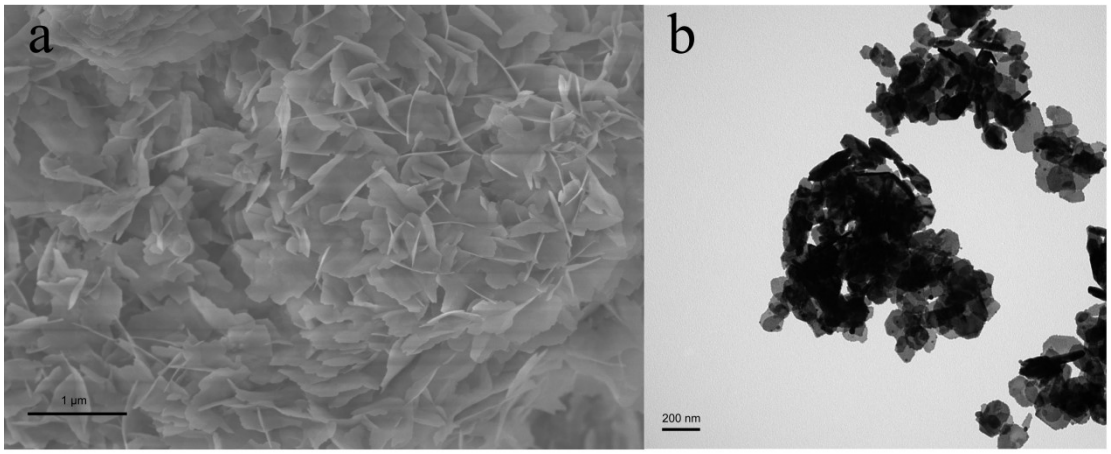

Fig. S2. The SEM image of Ag/Bi_2O_3.

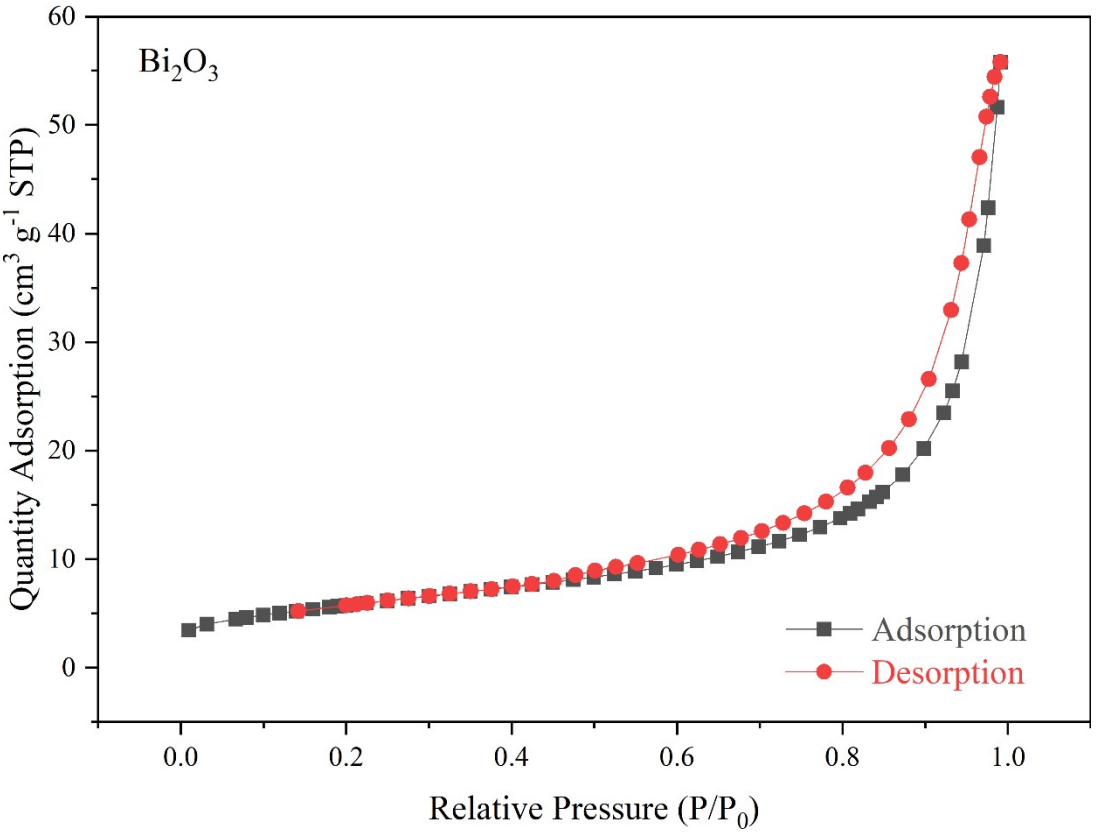

Fig. S3. Nitrogen adsorption and desorption isotherm curves of Bi_2O_3.

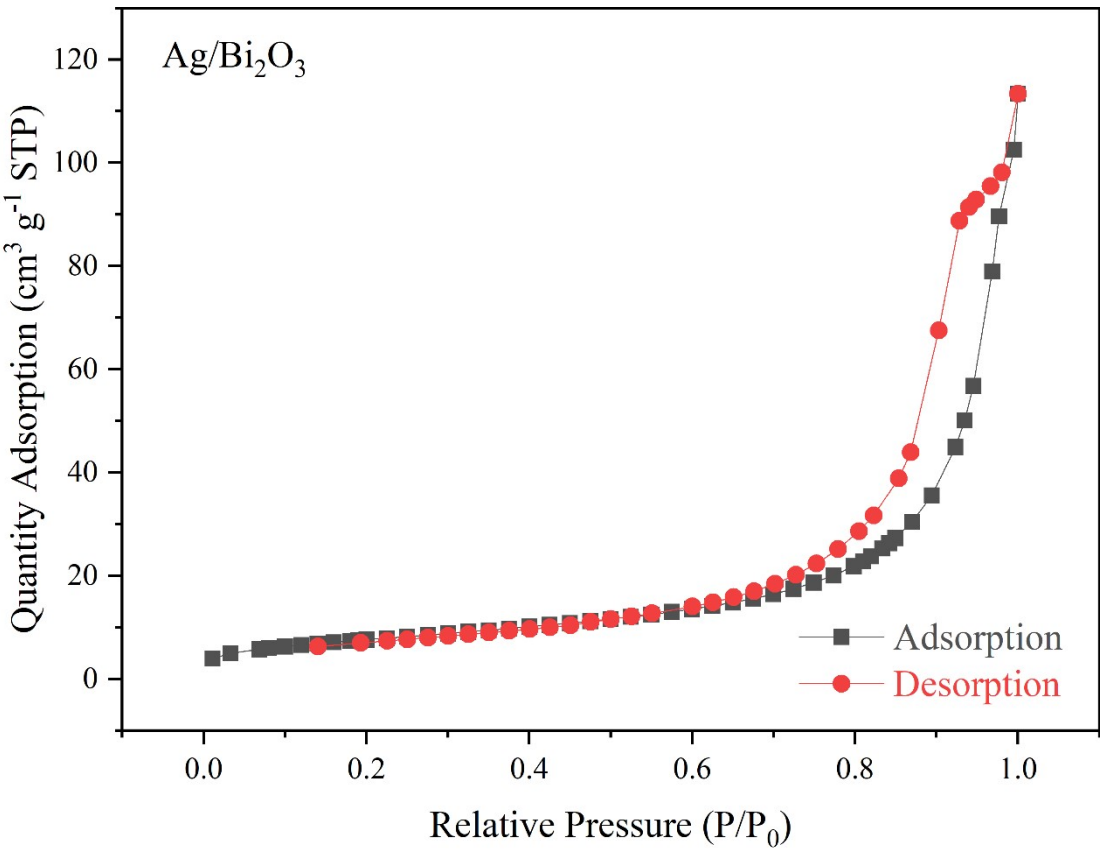

Fig. S4. Nitrogen adsorption and desorption isotherm curves of Ag/Bi_2O_3.

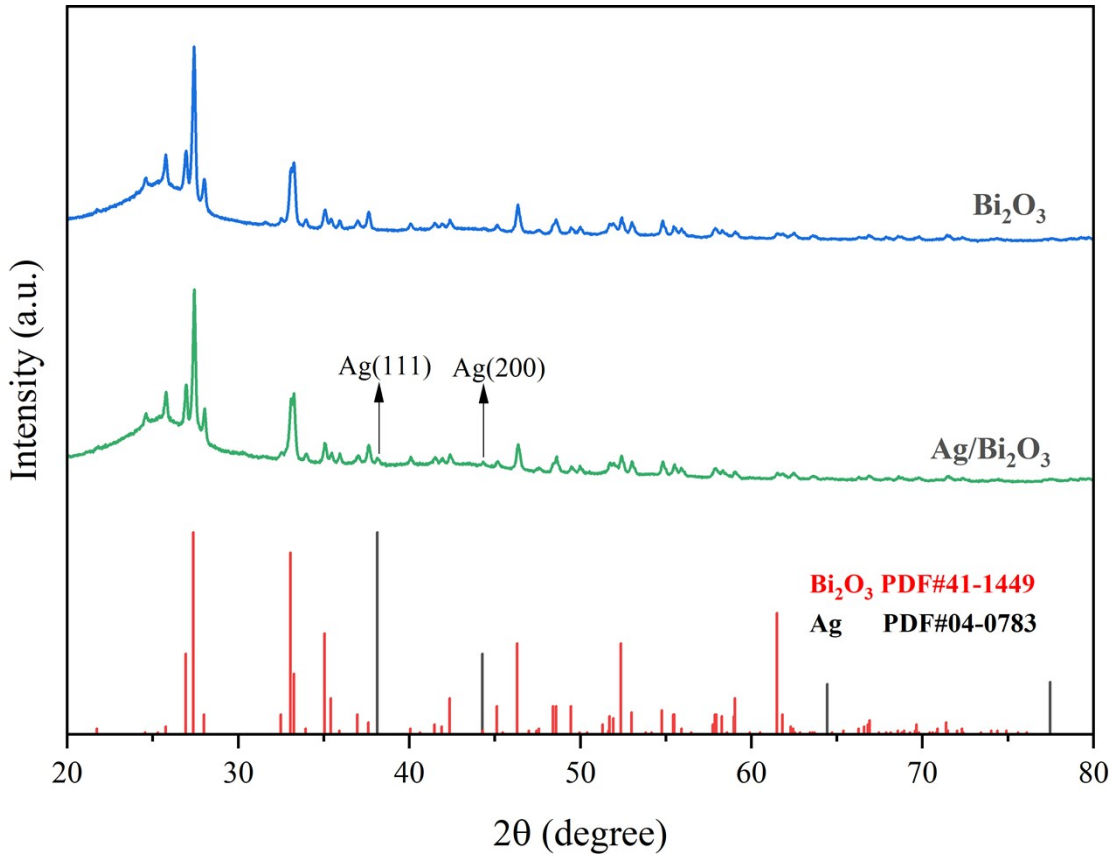

Fig. S5. XRD spectra of Bi_2O_3 and Ag/Bi_2O_3 on carbon paper.

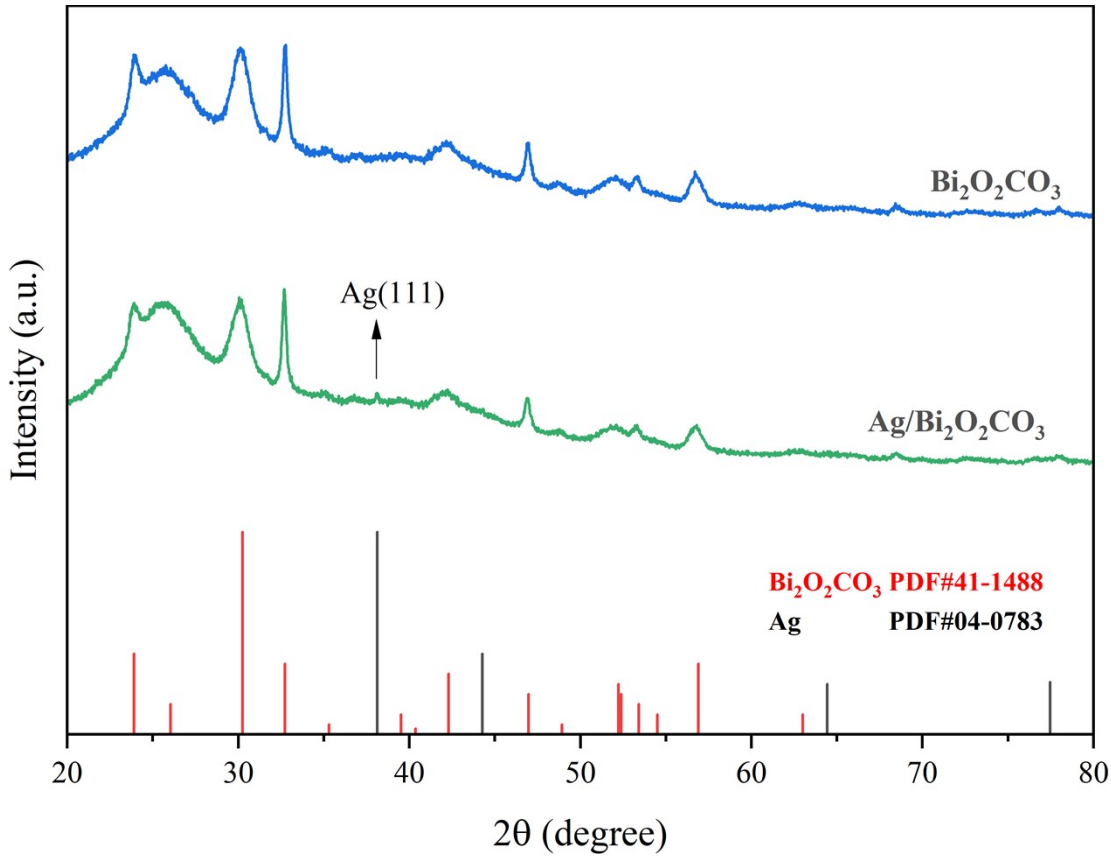

Fig. S6. XRD spectra of $Bi_2O_2CO_3$ and $Ag/Bi_2O_2CO_3$ on carbon paper.

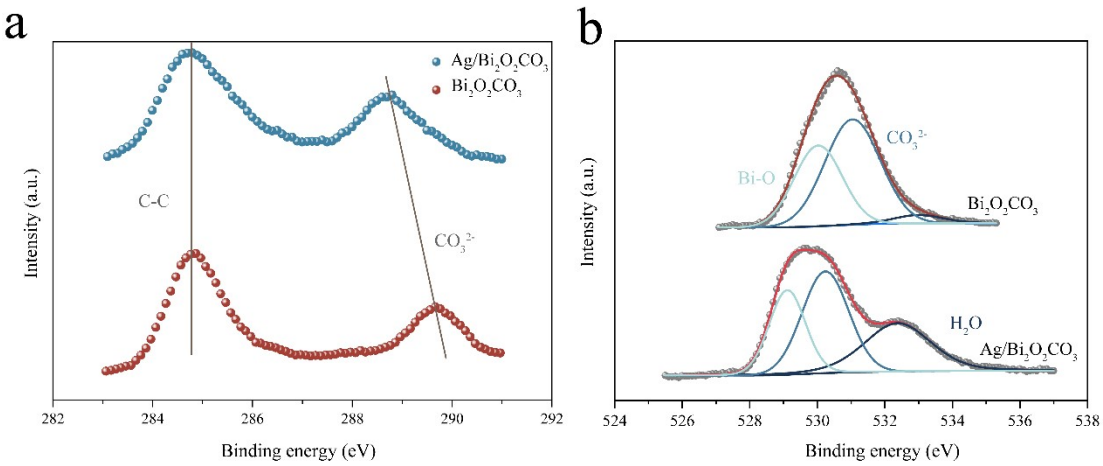

Fig. S7. The (a) C 1s and (b) O 1s XPS spectrum of $Bi_2O_2CO_3$ and $Ag/Bi_2O_2CO_3$.

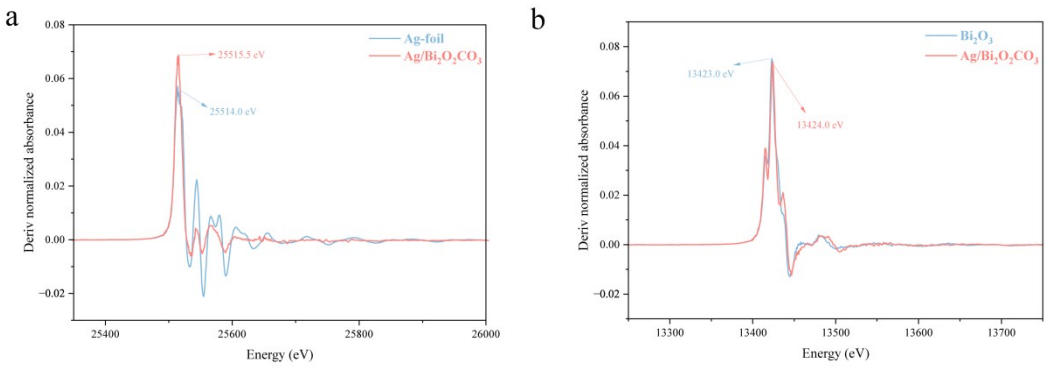

Fig. S8. (a) Differential curves of Ag K-edge XANES of Ag-foil and $Ag/Bi_2O_2CO_3$. (b) Differential curves of Bi L_3-edge XANES of Bi_2O_3 and $Ag/Bi_2O_2CO_3$.

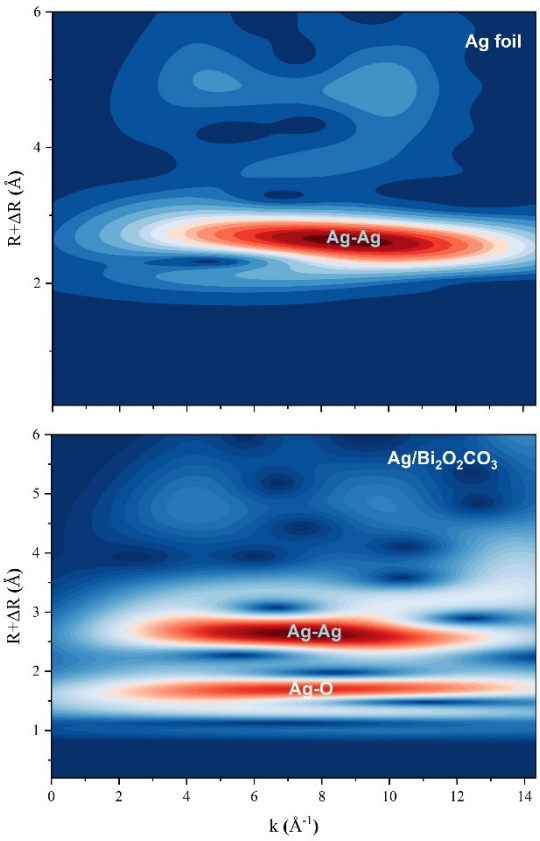

Fig. S9. Ag K-edge EXAFS wavelet transform plots of Ag foil and $Ag/Bi_2O_2CO_3$.

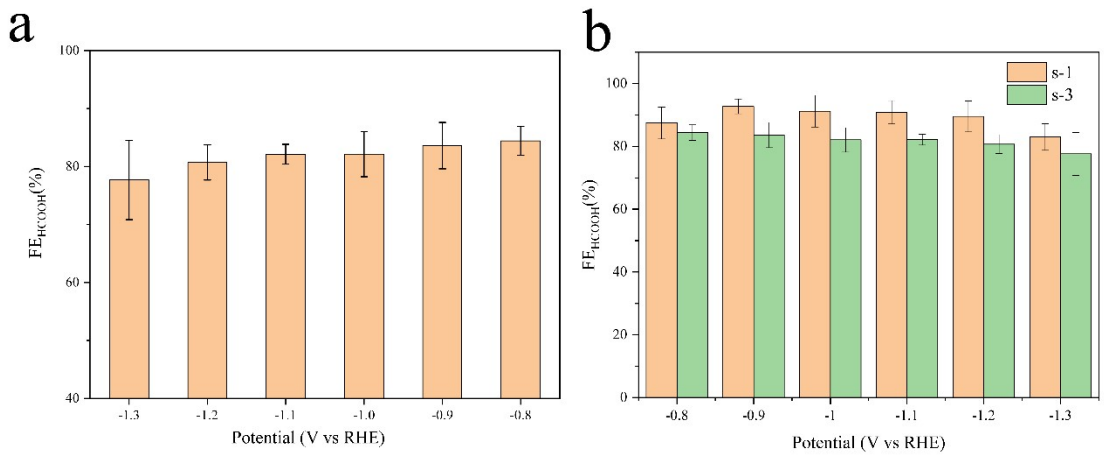

Fig. S10. (a) The FE_{HCOOH} of $Bi_2O_2CO_3$ at different applied potential. (b) The FE_{HCOOH} of s-1 and s-3 at different applied potential.

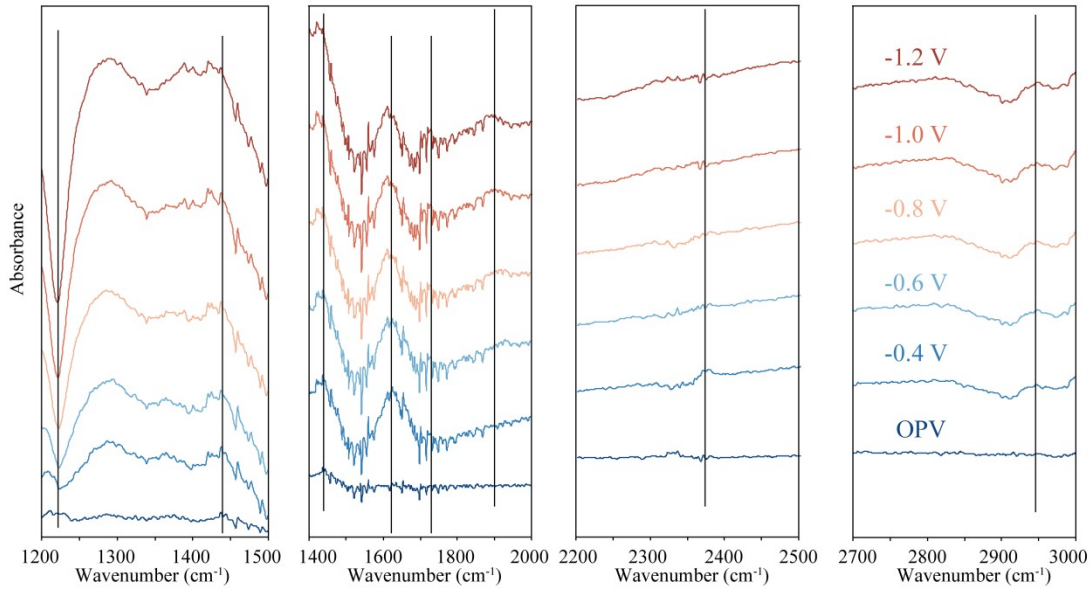

Fig. S11. Enlarged in situ infrared spectrum of $Ag/Bi_2O_2CO_3$.

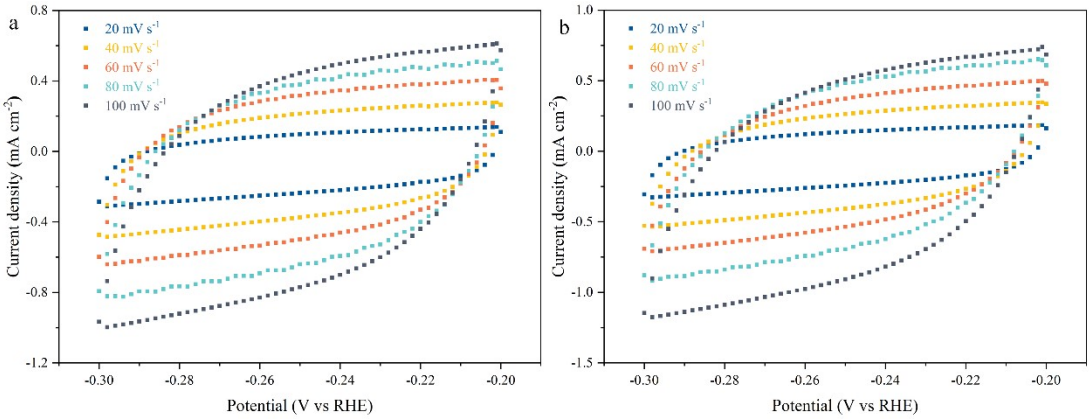

Fig. S12. Cyclic voltammogram scans of (a) $Bi_2O_2CO_3$ and (b) $Ag/Bi_2O_2CO_3$ measured in a narrow potential window where only double-layer charging and discharging occur at various scan rates.

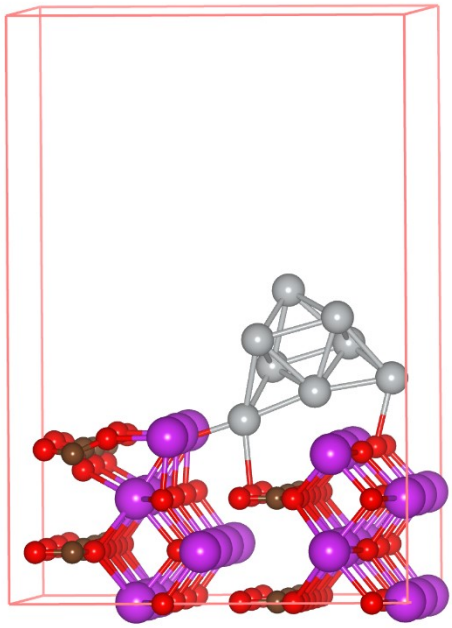

Fig. S13. The optimized model of $Ag/Bi_2O_2CO_3$. The brown, red, grey, and purple balls represent C, O, Ag, and Bi atoms, respectively.

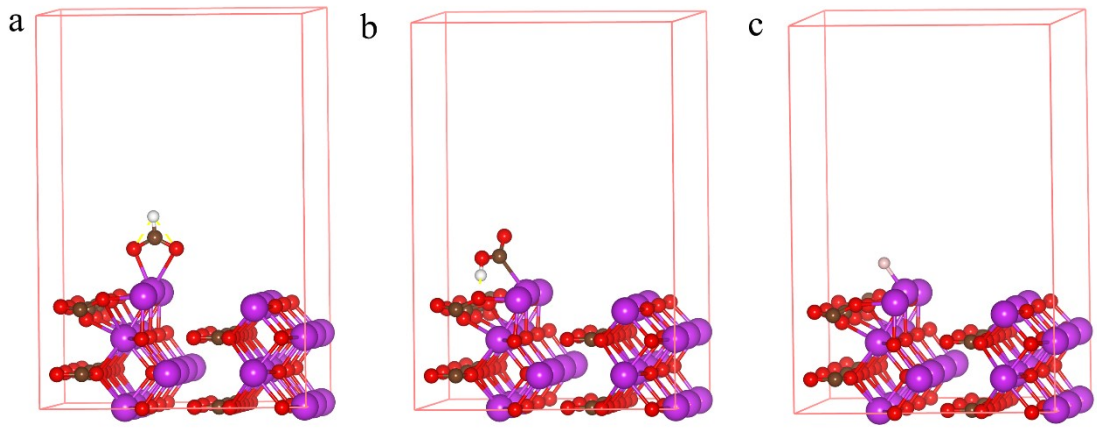

Fig. S14. The geometrical configuration of *OCHO (a), *COOH (b), and *H (c) over $Bi_2O_2CO_3$. The white, blown, red, and purple balls represent H, C, O, and Bi atoms, respectively.

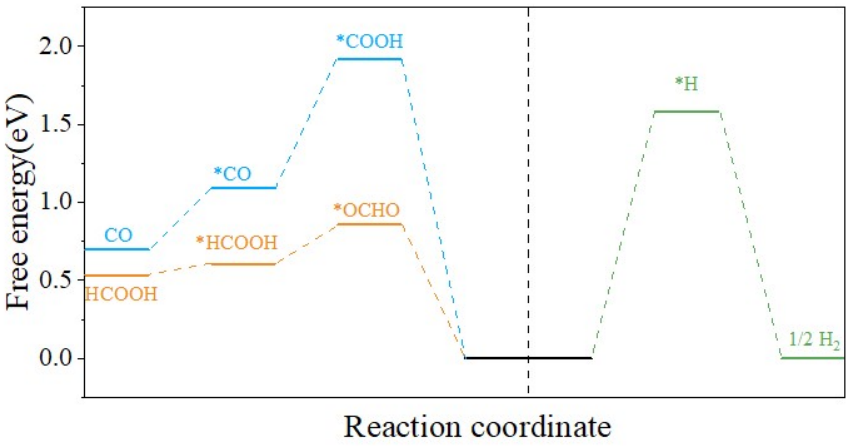

Fig. S15. Calculated free energy diagram of HCOOH, CO, and H_2 formation over $Bi_2O_2CO_3$(100) surface.

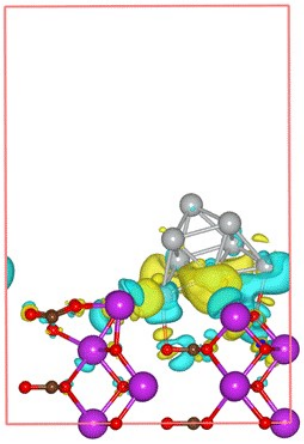

Fig. S16. Differential charge density from first-principles simulations illustrates the increase (olive color) and decrease (cyan color) of electron distributions; the isosurface value of the color region is 0.001 e per $Å^3$.

Table S1. The reported electrocatalysts for CO_2RR towards HCOOH.

Catalysts	**Electrolyte**	**FE_{HCOOH}**	**Ref.**
Ta-Pb	0.5M $NaHCO_3$	96.4%	R[5]
In-SAs/NC	0.5M $KHCO_3$	96%	R[6]
SnO_2/NSC	0.5M $KHCO_3$	94.4%	R[7]
Sb SA/NC	0.5M $KHCO_3$	94%	R[8]

Table S2. The reported Bi-based electrocatalysts for CO_2RR towards HCOOH.

Catalysts	Electrolyte	Potential window for FE_{HCOOH} > 90% (V vs RHE)	Ref.
Bi/Bi_2O_3-CP	0.5M $KHCO_3$	-0.85 — -1.0	R[9]
Bi-Sn aerogel	0.1M $KHCO_3$	-0.9 — -1.2	R[10]
Bi-300 nanosheets	0.5M $KHCO_3$	-0.7 — -0.8	R[11]
Bi-ene	0.5M $KHCO_3$	-0.7 — -1.2	R[12]
Bi_2O_3NSs@MCCM	0.1M $KHCO_3$	-1.05 — -1.35	R[13]
AgBi-500	0.1M $KHCO_3$	-0.7 — -1.0	R[14]
Bi-Sn/CF	0.5M $KHCO_3$	-1.14 — -1.24	R[15]
mpBi	0.5M $NaHCO_3$	-0.75 — -1.0	R[16]
Bi NTs	0.5M $KHCO_3$	-0.8 — -1.25	R[17]
Bi NSs	0.5M $KHCO_3$	-0.75 — -1.05	R[18]
$Ag/Bi_2O_2CO_3$	0.5M $KHCO_3$	-0.8 — -1.3	This work

Table S3. The content of Ag detected from ICP-AES measurement.

sample	s-1	s-2	s-3
Ag Content (wt.%)	0.358	0.384	2.928

Reference

[1] Y. Wang, Z. Wang, C.-T. Dinh, J. Li, A. Ozden, M. Golam Kibria, A. Seifitokaldani, C.-S. Tan, C.M. Gabardo, M. Luo, H. Zhou, F. Li, Y. Lum, C. McCallum, Y. Xu, M. Liu, A. Proppe, A. Johnston, P. Todorovic, T.-T. Zhuang, D. Sinton, S.O. Kelley, E.H. Sargent, Catalyst synthesis under CO2 electroreduction favours faceting and promotes renewable fuels electrosynthesis, Nat Catal. 3 (2020) 98–106. https://doi.org/10.1038/s41929-019-0397-1.

[2] G. Kresse, J. Hafner, *Ab initio* molecular dynamics for open-shell transition metals, Phys. Rev. B. 48 (1993) 13115–13118. https://doi.org/10.1103/PhysRevB.48.13115.

[3] G. Kresse, D. Joubert, From ultrasoft pseudopotentials to the projector augmented-wave method, Phys. Rev. B. 59 (1999) 1758–1775. https://doi.org/10.1103/PhysRevB.59.1758.

[4] J.P. Perdew, K. Burke, M. Ernzerhof, Generalized Gradient Approximation Made Simple, Phys. Rev. Lett. 77 (1996) 3865–3868. https://doi.org/10.1103/PhysRevLett.77.3865.

[5] Y. Shi, Y. Ji, J. Long, Y. Liang, Y. Liu, Y. Yu, J. Xiao, B. Zhang, Unveiling hydrocerussite as an electrochemically stable active phase for efficient carbon dioxide electroreduction to formate, Nat Commun. 11 (2020) 3415. https://doi.org/10.1038/s41467-020-17120-9.

[6] H. Shang, T. Wang, J. Pei, Z. Jiang, D. Zhou, Y. Wang, H. Li, J. Dong, Z. Zhuang, W. Chen, D. Wang, J. Zhang, Y. Li, Design of a Single-Atom Indium $^{\delta+}$ –N $_4$ Interface for Efficient Electroreduction of CO $_2$ to Formate, Angew. Chem. Int. Ed. 59 (2020) 22465–22469. https://doi.org/10.1002/anie.202010903.

[7] L.-P. Yuan, W.-J. Jiang, X.-L. Liu, Y.-H. He, C. He, T. Tang, J. Zhang, J.-S. Hu, Molecularly Engineered Strong Metal Oxide–Support Interaction Enables Highly Efficient and Stable CO $_2$ Electroreduction, ACS Catal. 10 (2020) 13227–13235. https://doi.org/10.1021/acscatal.0c03831.

[8] Z. Jiang, T. Wang, J. Pei, H. Shang, D. Zhou, H. Li, J. Dong, Y. Wang, R. Cao, Z. Zhuang, W. Chen, D. Wang, J. Zhang, Y. Li, Discovery of main group single Sb–N $_4$ active sites for CO $_2$ electroreduction to formate with high efficiency, Energy Environ. Sci. 13 (2020) 2856–2863. https://doi.org/10.1039/D0EE01486A.

[9] D. Wu, G. Huo, W. Chen, X.-Z. Fu, J.-L. Luo, Boosting formate production at high current density from CO2 electroreduction on defect-rich hierarchical mesoporous Bi/Bi2O3 junction nanosheets, Applied Catalysis B: Environmental. 271 (2020) 118957. https://doi.org/10.1016/j.apcatb.2020.118957.

[10] Z. Wu, H. Wu, W. Cai, Z. Wen, B. Jia, L. Wang, W. Jin, T. Ma, Engineering Bismuth–Tin Interface in Bimetallic Aerogel with a 3D Porous Structure for Highly Selective Electrocatalytic CO $_2$ Reduction to HCOOH, Angew. Chem. Int. Ed. 60 (2021) 12554–12559. https://doi.org/10.1002/anie.202102832.

[11] L. Yi, J. Chen, P. Shao, J. Huang, X. Peng, J. Li, G. Wang, C. Zhang, Z. Wen, Molten-Salt-Assisted Synthesis of Bismuth Nanosheets for Long-term Continuous Electrocatalytic Conversion of CO $_2$ to Formate, Angew. Chem. Int. Ed. 59 (2020) 20112–20119. https://doi.org/10.1002/anie.202008316.

[12] C. Cao, D. Ma, J. Gu, X. Xie, G. Zeng, X. Li, S. Han, Q. Zhu, X. Wu, Q. Xu, Metal–Organic Layers Leading to Atomically Thin Bismuthene for Efficient Carbon Dioxide Electroreduction to Liquid Fuel, Angew. Chem. Int. Ed. 59 (2020) 15014–15020. https://doi.org/10.1002/anie.202005577.

[13] S. Liu, X.F. Lu, J. Xiao, X. Wang, X.W. (David) Lou, Bi $_2$ O $_3$ Nanosheets Grown on Multi-Channel Carbon Matrix to Catalyze Efficient CO $_2$ Electroreduction to HCOOH, Angew. Chem. Int. Ed. 58 (2019) 13828–13833. https://doi.org/10.1002/anie.201907674.

[14] J. Zhou, K. Yuan, L. Zhou, Y. Guo, M. Luo, X. Guo, Q. Meng, Y. Zhang, Boosting Electrochemical Reduction of CO $_2$ at a Low Overpotential by Amorphous Ag-Bi-S-O Decorated Bi ^{0} Nanocrystals, Angew. Chem. Int. Ed. 58 (2019) 14197–14201. https://doi.org/10.1002/anie.201908735.

[15] G. Wen, D.U. Lee, B. Ren, F.M. Hassan, G. Jiang, Z.P. Cano, J. Gostick, E. Croiset, Z. Bai, L. Yang, Z. Chen, Orbital Interactions in Bi-Sn Bimetallic Electrocatalysts for Highly Selective Electrochemical CO $_2$ Reduction toward Formate Production, Adv. Energy Mater. 8 (2018) 1802427. https://doi.org/10.1002/aenm.201802427.

[16] H. Yang, N. Han, J. Deng, J. Wu, Y. Wang, Y. Hu, P. Ding, Y. Li, Y. Li, J. Lu, Selective CO $_2$ Reduction on 2D Mesoporous Bi Nanosheets, Adv. Energy Mater. 8 (2018) 1801536. https://doi.org/10.1002/aenm.201801536.

[17] K. Fan, Y. Jia, Y. Ji, P. Kuang, B. Zhu, X. Liu, J. Yu, Curved Surface Boosts Electrochemical CO $_2$ Reduction to Formate via Bismuth Nanotubes in a Wide Potential Window, ACS Catal. 10 (2020) 358–364. https://doi.org/10.1021/acscatal.9b04516.

[18] Dan Wang, K. Chang, Y. Zhang, Y. Wang, Q. Liu, Z. Wang, D. Ding, Y. Cui, C. Pan, Y. Lou, Y. Zhu, Y. Zhang, Unravelling the electrocatalytic activity of bismuth nanosheets towards carbon dioxide reduction: Edge plane versus basal plane, Applied Catalysis B: Environmental. 299 (2021) 120693. https://doi.org/10.1016/j.apcatb.2021.120693.